

Devil is in the Uniformity: Exploring Diverse Learners within Transformer for Image Restoration

Shihao Zhou^{1,2} Dayu Li¹ Jinshan Pan³ Juncheng Zhou¹ Jinglei Shi¹ Jufeng Yang^{1,2}

¹ VCIP & TMCC & DISec, College of Computer Science, Nankai University

² Nankai International Advanced Research Institute (SHENZHEN·FUTIAN)

³ School of Computer Science and Engineering, Nanjing University of Science and Technology

zhoushihao96@mail.nankai.edu.cn, ldy030911@gmail.com, sdluran@gmail.com

2112612@mail.nankai.edu.cn, jinglei.shi@nankai.edu.cn, yangjufeng@nankai.edu.cn

Abstract

Transformer-based approaches have gained significant attention in image restoration, where the core component, i.e., Multi-Head Attention (MHA), plays a crucial role in capturing diverse features and recovering high-quality results. In MHA, heads perform attention calculation independently from uniform split subspaces, and a redundancy issue is triggered to hinder the model from achieving satisfactory outputs. In this paper, we propose to improve MHA by exploring diverse learners and introducing various interactions between heads, which results in a **Hierarchical multi-head atTeNtion driven Transformer model**, termed **HINT**, for image restoration. **HINT** contains two modules, i.e., the **Hierarchical Multi-Head Attention (HMHA)** and the **Query-Key Cache Updating (QKCU)** module, to address the redundancy problem that is rooted in vanilla MHA. Specifically, HMHA extracts diverse contextual features by employing heads to learn from subspaces of varying sizes and containing different information. Moreover, QKCU, comprising intra- and inter-layer schemes, further reduces the redundancy problem by facilitating enhanced interactions between attention heads within and across layers. Extensive experiments are conducted on **12 benchmarks across 5 image restoration tasks**, including low-light enhancement, dehazing, desnowing, denoising, and deraining, to demonstrate the superiority of **HINT**. **The source code will be available at <https://github.com/joshyZhou/HINT>.**

1. Introduction

The Transformer-based frameworks [19, 59] achieve promising performance in the field of image restoration. The success of this paradigm is rooted in the self-attention mechanism (SA) modeling non-local relations of pixels, which is crucial for recovering the global structure of the image. Many works pay attention to develop efficient SA

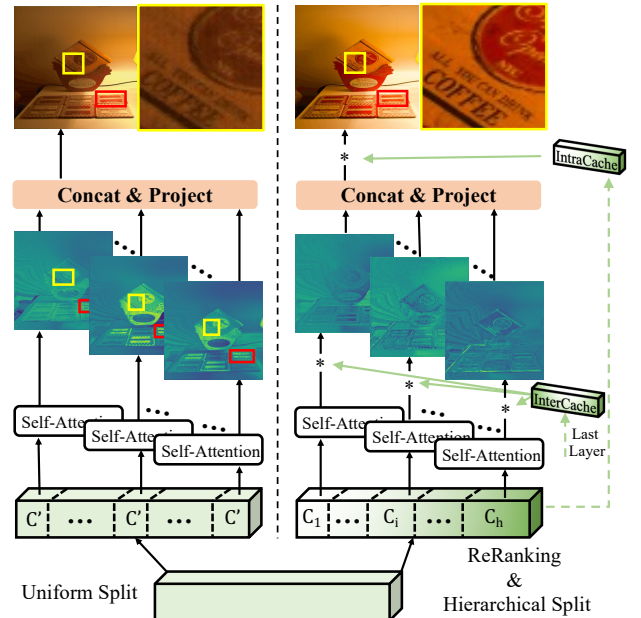


Figure 1. Comparisons between the vanilla MHA [2, 37, 82] (Left) and the proposed HMHA equipped with the QKCU module (Right), for the low-light enhancement task. The standard MHA assigns h heads with subspaces of the same size (C'), and each head performs attention calculation independently. As a result, these heads intend to focus on the same regions (red boxes) and neglect the restoration of some degraded areas (yellow boxes), leading to an unsatisfactory output (losing details and introducing blur effect). In contrast, HMHA implements the reranking operation before a hierarchical subspace split, which encourages the model to learn diverse representative features. The QKCU enhances interactions between heads via intra-/inter-layer ways, modulating predicted features in HMHA and leading to better outputs.

variants for high-quality outputs [37, 57, 82]. While it is worth noting that multi-head attention (MHA), employing multiple heads to perform self-attention computation in parallel from uniform split subspace, serves as the key fundamental component in embracing high computational efficiency and enhancing the diversity of the captured features.

The conventional MHA mechanism has a drawback of the redundancy issue. Some researches [48, 49, 64], in the field of NLP, have pointed out that specialized heads contribute most to the final decision while others can be pruned. In this paper, we demonstrate that this problem exists in the restoration tasks, and further find out that the redundancy issue can be traced to the focus on the same region by different heads. As shown in Figure 1, the standard MHA mechanism assigns h heads with subspaces of the same dimension (C'), where each head performs attention calculations in parallel and independently of the others. The visualized features from different heads disclose the problem of the vanilla MHA - that is, the inclination to pay attention to the same region (red boxes) which is redundant, and neglect of restoration on some degraded areas (yellow boxes) which causes unpleasant outputs.

To address this limitation, we improve the MHA from two perspectives. **First**, the heads learn from subspaces of uniform size, which contain similar information, leading to the problem of focusing on the same regions. Intuitively, to mitigate this issue, we introduce a ranking paradigm in terms of channel similarity before a hierarchical subspace splitting. In this way, each subspace contains information independent from others, and their sizes are different. This design explores heads as diverse learners, resulting in a hierarchical Multi-Head Attention module, namely HMHA, to replace the vanilla counterpart. It is capable of extracting diverse representative features, compared to the conventional MHA. **Second**, a lack of collaboration between heads makes the redundancy problem worse. We propose to enhance interactions between heads in intra- and inter-layer schemes through a Query-Key Cache Updating (QKCU) mechanism. Specifically, the intra-layer cache serves as a gating module, enhancing useful information in aggregated features that are captured by heads. On the other hand, the inter-layer cache emphasizes modulating the calculated attention score of each head, using history attention scores. Both intra- and inter- modulation are dependent on inputs, which improve the capability of HMHA to learn diverse contextual representations. Building upon the two key components, i.e., HMHA and QKCU, we propose HINT, a **H**ierarchical multi-head **a**ttention driven **T**ransformer model for image restoration.

Overall, we summarize the contributions of this work:

- We present HINT, a **H**ierarchical multi-head **a**ttention driven **T**ransformer model for removing undesired degradations from images. HINT demonstrates the effect of exploring diverse learners in Multi-Head Attention (MHA) and enhancing interactions via inter- and intra-layer ways for the problem of image restoration.
- HINT introduces Hierarchical Multi-Head Attention (HMHA), which alleviates the redundancy issue in standard MHA by enabling the model to learn distinctive

contextual features from different subspaces. Additionally, HINT incorporates the Query-Key Cache Updating (QKCU) mechanism, combining intra- and inter-layer schemes to enhance interaction between heads.

- Extensive qualitative and quantitative evaluations are conducted on **12** benchmarks for **5** typical image restoration tasks: low-light enhancement, dehazing, desnowing, denoising, and deraining, where HINT performs favorably against state-of-the-art algorithms in terms of restored image quality and model complexity.

2. Related Work

2.1. Image Restoration

Capturing images in unsatisfactory environments often results in low-quality outputs, negatively impacting downstream tasks [5, 20, 28]. Image restoration offers a plausible solution by recovering clear images from undesired degradations, e.g., haze [25, 32, 56], rain streaks [22, 51, 66], and low-light [2, 70, 75]. Over the past decades, the research community has witnessed the paradigm shift from conventional hand-crafted approaches [9, 21] to learning-based CNN models [38, 45, 79]. To achieve improved restoration performance, various efficient modules and advanced architecture designs have been proposed. Among these, residual feature learning [23, 40, 86] with skip connection, encoder-decoder architecture [10, 30, 80] for hierarchical representations, and attention mechanisms [17, 55, 83] to emphasize important signals have become the popular ingredients.

In recent years, Transformer-based models [59] have been adapted for low-level tasks, achieving significant advancements across various image restoration tasks [2, 57, 74]. IPT [3] is a pioneering work that applies the vision Transformer [19] to low-level tasks, and obtains surprising results. The quadratic complexity of vanilla self-attention hinders it from applying high-resolution inputs, prompting researchers to explore solutions for reducing computational loads. To address this, Restormer [82] computes attention scores along channel dimension. Another approach is window-based attention [43], which is adopted by models such as Uformer [69] and SwinIR [37]. Although these attention mechanisms successfully alleviate the computational burden, they still rely on the vanilla MHA [59], which incurs redundancy issue [47, 49, 73] and further limits the representation capacity of the model.

2.2. Multi-Head Attention

As a fundamental component of the Transformer, MHA plays a crucial role in capturing diverse relationships and achieving impressive performance in practice. Unfortunately, it is well known in the research community that not all heads contribute equally to the given task [60]. Previous works have attempted to address this by incorporating

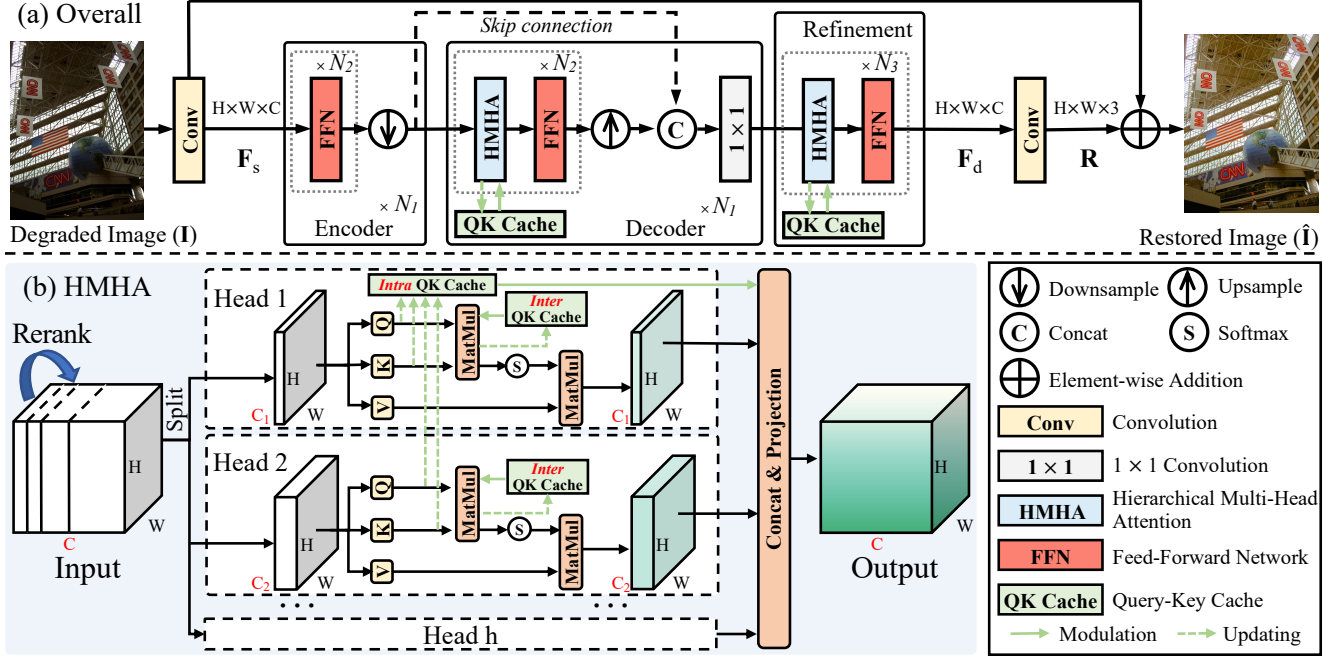


Figure 2. Illustration of the proposed Hierarchical multi-head attention driven Transformer model (HINT). (a) Overview architecture of the proposed HINT. (b) Hierarchical Multi-Head Attention (HMHA) mechanism.

interaction or collaboration between heads [1, 35, 85], however, the expressive power gained from these methods remains limited, as the heads still operate independently [73]. Another potential remedy is to modulate the query, key, and value projections of heads [12, 41]. While this modifies the underlying information flow, it lacks adaptability to inputs due to its static nature [73]. More recently, the community has explored dynamically modulating attention scores [48, 54, 64], which ensures improvement of expressive power without introducing much computational loads.

In this study, towards solving the image restoration problem, we build upon the basic idea of modulating attention scores [48, 73], while further mitigating the limited expressive power issue that is rooted in the vanilla MHA. Specifically, standard MHA assigns each head with subspaces using the same dimension size [3, 37, 82], limiting the ability of the heads to learn distinctive features and resulting in redundancy. In contrast, we propose to learn hierarchical representations using HMHA that extracts diverse contextual information from heads using different dimensional subspaces. Additionally, we introduce the QKCU mechanism, incorporating both intra- and inter-layer schemes, to enhance interaction among heads. Unlike existing restoration methods to implement modulation of attention scores in a static projection way [8, 88], HINT makes the modulation dynamic, achieving better model expressiveness.

3. Method

Overall Pipeline. As illustrated in Figure 2, the proposed HINT follows an encoder-decoder architecture. Given a de-

graded input $I \in \mathbb{R}^{H \times W \times 3}$, a convolutional layer is first used to extract the shallow feature $F_s \in \mathbb{R}^{H \times W \times C}$, where H , W , and C represent the height, width and channel dimension, respectively. The shallow feature is then processed through the N_1 -level restoration pipeline to produce a deep feature $F_d \in \mathbb{R}^{H \times W \times C}$. At each level of both the encoder and decoder, there are N_2 basic blocks, along with a convolution layer for down-sampling or up-sampling. Following prior works [29, 88, 89], we adopt an asymmetric design, which omits the self-attention mechanism in the encoder part, to boost the restoration performance. Thus, the basic block in the encoder consists only of a Feed-Forward Network (FFN) [82], while in the decoder, the block includes both the proposed HMHA and an FFN. We employ skip connection operation with 1×1 convolution to take advantage of features from the encoder in the decoder layers. After that, a refinement stage, consisting of N_3 basic blocks, is developed to further enhance the learned features. Finally, a 3×3 convolution layer processes the deep feature F_d to generate the residual image $R \in \mathbb{R}^{H \times W \times 3}$. The restored image is obtained by adding the residual image to the degraded one, i.e., $\hat{I} = I + R$.

3.1. Hierarchical Multi-head Attention

Standard MHA assigns each head with a subspace of the same size containing similar information, which hampers the ability to learn distinctive features, leading to redundancy. To address this, HINT forms the HMHA to explore different dimensional subspaces, encouraging each head to learn diverse contextual information.

We begin by revisiting the scaled dot-product attention mechanism in MHA [59], which is adopted in mainstream approaches [37, 82, 88]. Given a normalized input tensor $\mathbf{X} \in \mathbb{R}^{H \times W \times C}$, the attention score is calculated as:

$$\text{Attention}(\mathbf{Q}, \mathbf{K}, \mathbf{V}) = \text{Softmax}\left(\frac{\mathbf{Q}\mathbf{K}^T}{\sqrt{d_k}}\right) \mathbf{V}, \quad (1)$$

$$\mathbf{Q} = \mathbf{X}\mathbf{W}_Q, \mathbf{K} = \mathbf{X}\mathbf{W}_K, \mathbf{V} = \mathbf{X}\mathbf{W}_V,$$

where $\mathbf{W}_Q \in \mathbb{R}^{C \times d_k}$, $\mathbf{W}_K \in \mathbb{R}^{C \times d_k}$, and $\mathbf{W}_V \in \mathbb{R}^{C \times d_v}$ are the linear projection matrices for the query (\mathbf{Q}), key (\mathbf{K}), and value (\mathbf{V}). Notably, for self-attention, the dimensions of key and value are equal, i.e., $d_k = d_v$.

The conventional MHA [19, 82] leverages multiple heads to perform scaled dot-product attention in parallel. By operating the attention function on different subspaces, the representation power of the model is supposed to be enhanced. Specifically, standard MHA adopts h heads to learn representations of $(\mathbf{Q}, \mathbf{K}, \mathbf{V})$ in different subspace, i.e., d_k/h . The MHA can be formally expressed as:

$$\text{MultiHead}(\mathbf{X}) = \text{Concat}(\mathbf{H}_1, \mathbf{H}_2, \dots, \mathbf{H}_h) \mathbf{W}_p, \quad (2)$$

$$\mathbf{H}_i = \text{Attention}(\mathbf{X}\mathbf{W}_Q^i, \mathbf{X}\mathbf{W}_K^i, \mathbf{X}\mathbf{W}_V^i),$$

where $\mathbf{W}_Q^i \in \mathbb{R}^{C \times d_k/h}$, $\mathbf{W}_K^i \in \mathbb{R}^{C \times d_k/h}$, and $\mathbf{W}_V^i \in \mathbb{R}^{C \times d_v/h}$ are the projection matrices for the i -th head. The output projection matrix $\mathbf{W}_p \in \mathbb{R}^{d_v \times d_{out}}$ aggregates the features captured by all heads.

To enhance the express power of MHA, we introduce a hierarchical representation learning process. To be specific, the proposed HMHA assign each head to a different dimensional subspace by splitting the channel space as $C = [C_1, C_2, \dots, C_h]$ with $C_1 \leq C_2 \leq \dots \leq C_h$. Before performing this split, we first rerank the channels based on their similarity to ensure that each head focuses on distinct semantic features. Each head then operates within its own subspace, performing dot-product attention in different subspace to capture diverse contextual information.

3.2. Query-Key Cache Updating Mechanism

The HMHA mechanism encourages multiple heads to learn features containing diverse contextual information, while these heads still work independently as conventional works [37, 82]. In this way, there is a lack of collaboration within the layer and across the entire model. As a result, the model is hindered from achieving optimal restoration performance. To mitigate this issue, we develop a QKCU mechanism that enhances interaction among heads, both within layers and across layers, as illustrated in Figure 3.

Intra Query-Key Cache Modulation & Updating. Given two input tensors, including the IntraCache $\mathbf{F}_{\text{intra}} \in \mathbb{R}^{C \times HW}$ and Output of HMHA $\mathbf{F}_{\text{out}} \in \mathbb{R}^{C \times HW}$, we begin by computing the sum of the two features $\mathbf{F}_{\text{intra}}^s =$

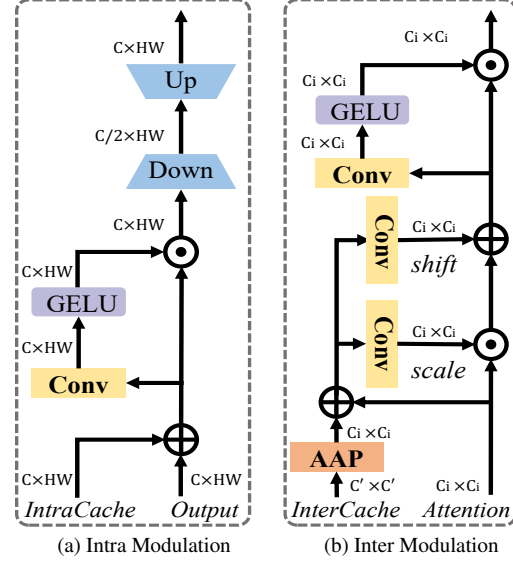


Figure 3. Query-Key Cache Updating Mechanism.

$\mathbf{F}_{\text{intra}} + \mathbf{F}_{\text{out}}$. To selectively retain the most informative elements within the flow of information, we introduce a gating mechanism, which can be formulated as:

$$\mathbf{F}_{\text{gated}} = \text{GELU}(\text{Conv}(\mathbf{F}_{\text{intra}}^s)) \odot \mathbf{F}_{\text{intra}}^s, \quad (3)$$

where $\mathbf{F}_{\text{gated}} \in \mathbb{R}^{C \times HW}$ is the result of the gating mechanism, \odot denotes element-wise multiplication, $\text{Conv}(\cdot)$ and $\text{GELU}(\cdot)$ are convolution operation and the GELU activation function [26], respectively. Then, we adapt this transformed feature via feature compression and rebuilding:

$$\mathbf{F}_{\text{intra}}^o = \text{Conv}_{\text{up}}(\text{Conv}_{\text{down}}(\mathbf{F}_{\text{gated}})), \quad (4)$$

where $\mathbf{F}_{\text{intra}}^o \in \mathbb{R}^{C \times HW}$ is the output feature after the modulation process, $\text{Conv}_{\text{up}}(\cdot)$ and $\text{Conv}_{\text{down}}(\cdot)$ are convolution operations that project the channel dimension into higher and lower levels, respectively. This design encourages the model to focus on the key features of the data.

Next, to update the Intra Query-Key Cache in each layer, we compute the sum of the Query (\mathbf{Q}) and Key (\mathbf{K}) projections for each head as follows:

$$\mathbf{F}^i = \mathbf{Q}^i + \mathbf{K}^i, \quad (5)$$

$$\mathbf{F}_{\text{intra}} = \text{Concat}(\mathbf{F}^1, \dots, \mathbf{F}^h)$$

Inter Query-Key Cache Modulation & Updating. Given two input tensors, the InterCache $\mathbf{F}_{\text{inter}} \in \mathbb{R}^{C' \times C'}$ and the dot-product attention of query and key $\mathbf{F}_{\text{att}} \in \mathbb{R}^{C_i \times C_i}$, we first resize $\mathbf{F}_{\text{inter}}$ to obtain $\hat{\mathbf{F}}_{\text{inter}} \in \mathbb{R}^{C_i \times C_i}$. After that, we compute the modulation components by summing \mathbf{F}_{att} and the resized feature map $\hat{\mathbf{F}}_{\text{inter}}$, resulting in: $\mathbf{F}_{\text{inter}}^s = \mathbf{F}_{\text{att}} + \hat{\mathbf{F}}_{\text{inter}}$. We then calculate ‘scale’ and ‘shift’ components for pixel-wise modulation:

$$\mathbf{F}_{\text{shift}} = \mathbf{F}_{\text{inter}}^s \mathbf{W}_{\text{shift}}, \mathbf{F}_{\text{scale}} = \mathbf{F}_{\text{inter}}^s \mathbf{W}_{\text{scale}}, \quad (6)$$

$$\mathbf{F}_m = \mathbf{F}_{\text{scale}} \odot \mathbf{F}_{\text{att}} + \mathbf{F}_{\text{shift}},$$

where $\mathbf{F}_m \in \mathbb{R}^{C_i \times C_i}$ is the modified feature map, $\mathbf{W}_{\text{scale}}$ and $\mathbf{W}_{\text{shift}}$ are projection matrices that learned for $\mathbf{F}_{\text{scale}} \in \mathbb{R}^{C_i \times C_i}$ and $\mathbf{F}_{\text{shift}} \in \mathbb{R}^{C_i \times C_i}$ components, respectively. Similarly, this feature is further transformed via a gating mechanism, which can be defined as:

$$\mathbf{F}_{\text{inter}}^o = \text{GELU}(\text{Conv}(\mathbf{F}_m)) \odot \mathbf{F}_m, \quad (7)$$

where $\mathbf{F}_{\text{inter}}^o \in \mathbb{R}^{C_i \times C_i}$ is the output feature.

Next, to update the Inter Query-Key Cache across layers, we implement a layer-wise cache calculation process and refine the historical cache. The cache for the current layer:

$$\mathbf{F}_{\text{inter}}^l = \sum_{i=1}^h \text{R}(\mathbf{Q}^i \mathbf{K}^{iT}) C_i / C, \quad (8)$$

where $\text{R}(\cdot)$ is a function that resizes the feature map of each head to a uniform shape, and C_i / C is the assigned weight of each feature, with C being the total number of channels. Building upon the cache of the current layer, we progressively update the inter-layer cache as follows:

$$\mathbf{F}_{\text{inter}} = \alpha \mathbf{F}_{\text{inter}} + (1 - \alpha) \mathbf{F}_{\text{inter}}^l, \quad (9)$$

where the hyper-parameter α controls the degree of information flow within the inter-layer cache.

4. Experiments

In this section, we evaluate HINT on **12** benchmark datasets across **5** typical image restoration tasks, including low-light enhancement, dehazing, and desnowing, denoising, and deraining. Due to the limited space, additional results (image deraining and denoising) and detailed experimental settings are provided in the supplementary material.

4.1. Experimental Settings

Implementation Details. HINT consists of an encoder-decoder with $N_1 = 4$ levels, where both the encoder and decoder share the same block structure: $N_2 = [4, 6, 6, 6]$. At the 4-th level, the encoder and decoder block are unified into a bottleneck layer, following the design of [69]. The refinement stage contains $N_3 = 4$ blocks, and the embedding dimension C is set as 48. The number of attention heads is 4, with the dimensional ratio of [1, 2, 2, 3]. The reranking strategy adopted in HINT is built on Pearson correlation-based similarity. The hyper-parameter α in Equation (9) is experimentally set to 0.9. The AdamW optimizer is adopted to train HINT. The widely adopted loss functions [63, 89] are employed to constrain the model training.

Metrics. We employ the popular metrics, including peak signal-to-noise ratio (PSNR) [68] and structural similarity (SSIM), to evaluate the restored result with the reference image. Besides, the non-reference metric, i.e., MANIQA [76], is adopted to measure the restoration performance on real-world inputs. In the tables, we **highlight** and underline the best and second-best scores, respectively.

Table 1. Quantitative comparisons on LOL-v2 [77] for low-light enhancement. * indicates unsupervised methods.

Method	LOL-v2-real		LOL-v2-syn		Average	
	PSNR	SSIM	PSNR	SSIM	PSNR	SSIM
*EnGAN [27] (TIP'21)	18.23	0.617	16.57	0.734	17.4	0.676
*RUAS [39] (CVPR'21)	18.37	0.723	16.55	0.652	17.46	0.688
*QuadPrior [67] (CVPR'24)	20.48	0.811	16.11	0.758	18.30	0.785
KinD [87] (MM'19)	14.74	0.641	13.29	0.578	14.02	0.610
Uformer [69] (CVPR'22)	18.82	0.771	19.66	0.871	19.24	0.821
Restormer [82] (CVPR'22)	19.94	0.827	21.41	0.830	20.68	0.829
MIRNet [81] (ECCV'20)	20.02	0.820	21.94	0.876	20.98	0.848
Sparse [77] (TIP'21)	20.06	0.816	22.05	0.905	21.06	0.861
MambaIR [24] (ECCV'24)	21.25	0.831	25.55	0.929	23.40	0.880
SNR-Net [75] (CVPR'22)	21.48	0.849	24.14	0.928	22.81	0.889
IGDFormer [71] (PR'25)	22.73	0.833	25.33	0.937	24.03	0.885
Retinexformer [2] (ICCV'23)	22.80	0.840	25.67	0.930	24.24	0.885
MambaLLIE [72] (NeurIPS'24)	<u>22.95</u>	0.847	<u>25.87</u>	0.940	<u>24.41</u>	0.894
HINT (Ours)	23.11	0.884	27.17	0.950	25.14	0.917

4.2. Main Results

Low-Light Enhancement. We compare the proposed HINT with state-of-the-art low-light enhancement methods on the LOL-v2 dataset in Table 1. As one can see, HINT performs favorably against considered approaches in terms of PSNR and SSIM on both real and synthetic subsets. In particular, when averaged across both subsets, HINT achieves a significant 0.9 dB improvement on PSNR over Retinexformer [2], which is the first Transformer-based pipeline designed specifically for low-light enhancement. Compared to general image restoration schemes based on diverse architectures, e.g., CNN-based [81], Transformer-based [69, 82], and Mamba-based [24], HINT receives at least 1.74 dB gain. Notably, our model yields a remarkable 1.11 dB performance improvement on PSNR over the recent algorithm IGDFormer [71]. The qualitative comparison is depicted in Figure 4. In the top row, previous methods fall short of recovering satisfactory results. They either meet over-/under-exposed issue [39, 77] (Figure 4d and 4f) or struggle to restore the true colors [81, 82, 87] (Figure 4c, 4e and 4g). For the bottom case, the image restored by HINT is closer to the reference one, where other algorithms introduce noticeable blur patterns [77, 81, 82, 87] (Figure 4c, 4e, 4f, 4g), or cause a under-exposed problem [39] (Figure 4d).

Snow Removal. For image desnowing, we conduct experiments on the Snow100K [42] dataset. HINT archives the best PSNR score and a competitive SSIM result among all methods. To be specific, HINT provides a significant 1.64 dB boost on PSNR over the recent general restoration pipeline AST [88]. Additionally, compared to approaches [6, 7, 42] that are designed for desnowing, HINT showcases the superiority of better performance. Furthermore, compared to methods [36, 58] that are proposed to address adverse weather conditions, our method earns consistent benefits. For general restoration schemes, including CNN-based [4, 13, 14, 62] and Transformer-based [69, 88],

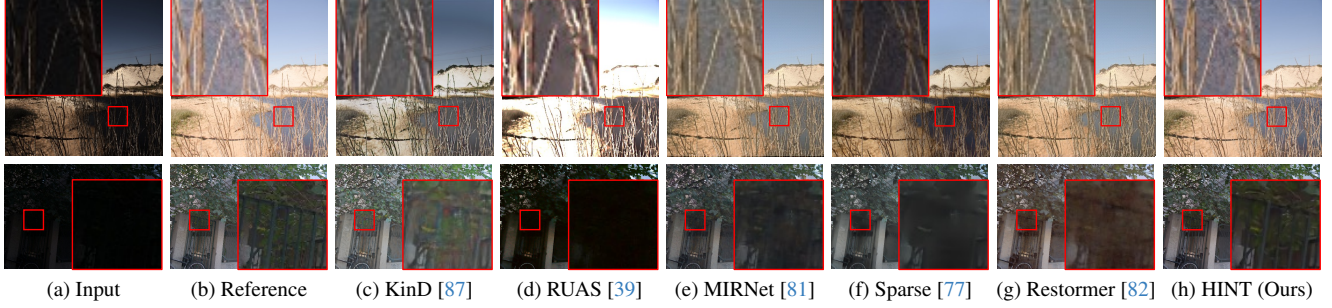


Figure 4. Qualitative results on LOL-v2 [77] for low-light enhancement. The top case is from the synthetic subset, whereas the bottom one is from the real subset. Compared to other techniques, HINT generates vivid images without introducing noticeable color distortion.



Figure 5. Qualitative results on Snow100K [42] for snow removal. HINT offers a clear result, while the images generated by other considered approaches remain noticeable snow artifacts.

Table 2. Quantitative results on Snow100K [42] for snow removal.

Method	JSTASR All in One Uformer DesnowNet HDCW TransWeather					
	ECCV'20 CVPR'20 CVPR'22 TIP'18 ICCV'21 CVPR'22					
	[6] [36] [69] [42] [7] [58]					
PSNR	23.12	26.07	29.80	30.50	31.54	31.82
SSIM	0.86	0.88	0.93	0.94	0.95	0.93
Method	NAFNet AST FocalNet SFNet ConvIR-S HINT					
	ECCV'22 CVPR'24 ICCV'23 ICLR'23 TPAMI'24					
	[4] [88] [13] [14] [62] (Ours)					
PSNR	32.41	32.50	33.53	33.79	33.79	34.14
SSIM	0.95	0.96	0.95	0.95	0.95	0.94

Table 3. Quantitative comparison on SOTS [33] for haze removal.

Method	EPDN FDGAN AirNet InstructIR Restormer NAFNet					
	CVPR'19 AAAI'20 CVPR'22 ECCV'24 CVPR'22 ECCV'22					
	[52] [18] [34] [11] [82] [4]					
PSNR	22.57	23.15	23.18	30.22	30.87	32.41
SSIM	0.863	0.921	0.900	0.959	0.969	0.970
Method	FSNet PromptIR DehazeFormer AdaIR NDR-Restore HINT					
	TPAMI'24 NeurIPS'23 TIP'23 ICLR'25 TIP'24					
	[15] [50] [56] [16] [78] (Ours)					
PSNR	31.11	31.31	31.78	31.80	31.96	32.24
SSIM	0.971	0.973	0.977	0.981	0.980	0.981

HINT shows at least a 0.35 dB performance boost on PSNR. The visual comparisons are shown in Figure 5, where HINT restores a clear result (Figure 5g). The desnowing techniques [6, 7] offer unsatisfactory outputs (Figure 5c and 5d). The results from Transformer-based approaches [69, 88] exhibit noticeable snow artifacts (Figure 5e and 5f).

Haze Removal. We perform image dehazing experiments on the SOTS [33] dataset, where 11 representative approaches are considered to make a comparison in Table 3. As can be seen, HINT outperforms all other methods on both PSNR and SSIM metrics. It is worth noting that, HINT surpasses all the methods [18, 52, 56], which are elaborately designed for dehazing, by at least 0.46 dB on PSNR.

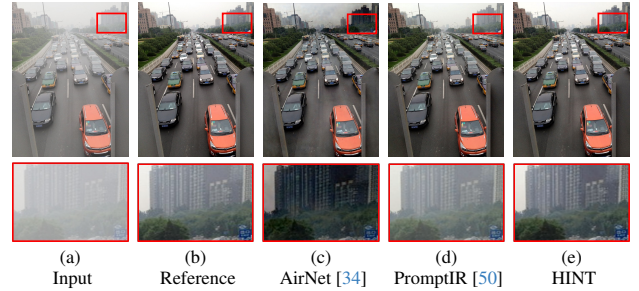


Figure 6. Qualitative results on SOTS [33] benchmark for haze removal. The image generated by HINT is closer to the reference one, compared to other methods.

When compared to image restoration pipelines (all-in-one paradigms [16, 50, 78] and general ones [4, 11, 15, 82]), HINT consistently shows advantages. Figure 6 illustrates the qualitative results. In comparison, other methods introduce either color distortion issue [34] (Figure 6c) or haze effect [50] (Figure 6d), while HINT restores a vivid result.

4.3. Analysis and Discussion

We have demonstrated that exploring the HMHA mechanism equipped with QKCU in a Transformer-based model brings benefits across several restoration tasks. Next, we further perform experiments to study the proposed modules and analyze the effect of each component. For ablation studies, various low-light enhancement models HINT are trained on the LOL-v2-syn subset [77]. To ensure fair comparisons, all models are trained under identical experimental settings, and the FLOPs/Runtimes are computed using 256×256 input images.

Effect of HMHA. To investigate whether the proposed HMHA enhances the capability of modeling diverse contextual information, we compare it with two representative variants, including (1) Window-based Multi-head Self-

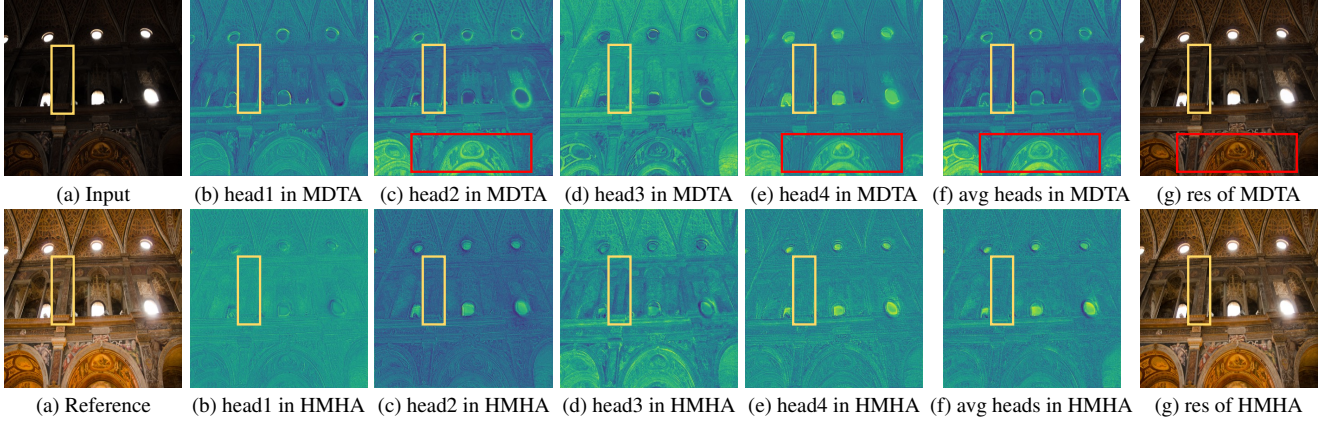


Figure 7. Feature Visualization. The top line exhibits the feature map of each head learned by MDTA, while the feature maps at the bottom illustrate the results of HMHA. The heads in MDTA intend to focus on the same regions (red boxes), whereas the counterparts in HMHA showcase superiority in learning representations from different subspaces. As a result, the model equipped with the proposed HMHA restores a pleasant image, which is closer to the reference one (yellow boxes).

Table 4. Ablation study for different self-attention mechanisms.

Model	W-MSA [69]	MDTA [82]	HMHA Ours
PSNR/SSIM	24.19/0.941	26.42/0.948	27.17/0.950

Table 5. Ablation study of HMHA.

	Ranking Strategy	Params	PSNR	SSIM
(a)	No-Ranking [82]	24.76	26.42	0.948
(b)	Random Shuffle [84]	24.87	26.54	0.949
(c)	HMHA (Ours)	24.87	27.17	0.950

Table 6. Ablation study of QKCU.

	IntraCache	InterCache	Params	PSNR	SSIM
(a)			21.34	26.47	0.949
(b)	✓		23.82	26.67	0.949
(c)		✓	22.39	26.72	0.949
(d)	✓	✓	24.87	27.17	0.950

Attention (W-MSA) [41], and (2) Multi-Dconv Head Transposed Attention (MDTA) [82]. The quantitative comparison is reported in Table 4. The model incorporating HMHA achieves the highest scores on both PSNR and SSIM metrics, outperforming other variants. Specifically, replacing HMHA with W-MSA or MDTA leads to significant performance drops of 2.98 dB and 0.75 dB, respectively. To investigate the effect of HMHA, we further visualize the feature maps learned by the heads in MDTA and HMHA, respectively. As shown in Figure 7, the heads in MDTA intend to focus on the same regions (indicated by red boxes), whereas the heads in HMHA showcase superiority in learning distinct representations from different subspaces. Consequently, the model with HMHA produces a result that is closer to the reference image (highlighted by yellow boxes).

We then show the effectiveness of the reranking strategy in HMHA for achieving discriminative representation

Table 7. Model efficiency analysis on LOL-v2-syn [66].

Method	IPT [3]	MIRNet [81]	Uformer [69]	Restormer [82]	HINT
FLOPs/G	6887	785	12.00	144.25	<u>126.92</u>
Parameters/M	115.3	31.76	5.29	26.13	<u>24.87</u>
Run-times/s	2.23	<u>0.19</u>	0.13	0.29	0.28
PSNR/dB	18.30	<u>21.94</u>	19.66	21.41	27.17

Table 8. Quantitative comparisons (MANIQA [76]) on real-world datasets. These results are all obtained from testing with their best LOL-v2-syn [66] weights. [↑ :Higher value denotes better quality]

Dataset	DICM [31]	MEF [46]	NPE [65]	VV [61]	Mean↑
SNR-Net [75]	0.465	0.527	0.480	0.239	0.428
Uformer [69]	0.526	0.634	<u>0.515</u>	<u>0.356</u>	<u>0.508</u>
Restormer [82]	<u>0.535</u>	<u>0.641</u>	0.491	<u>0.356</u>	0.507
Sparse [77]	0.458	0.532	0.324	0.341	0.413
HINT	0.583	0.642	0.547	0.448	0.555

in Table 5. When we replace the reranking strategy (Table 5c) with a random shuffle operation [84] (Table 5b), we observe a performance drop of 0.63 dB on PSNR. In contrast, compared to the model without any ranking mechanism (Table 5a), which is degraded to vanilla MHA [82], our HMHA achieves a significant 0.75 performance boost. These results highlight the positive impact of the reranking strategy in enhancing the expressive power of the model.

Effect of QKCU. To show the effectiveness of the proposed QKCU module, we conduct experiments on different variants in Table 6. Disabling either IntraCache or InterCache within QKCU results in performance declines of 0.45 dB and 0.5 dB, respectively, indicating the importance of these modules in restoring high-quality images. In total, the QKCU mechanism brings 0.7 dB performance gain with limited computation loads (16.5% in Parameters).

Model efficiency. We provide the comparison of model efficiency in terms of complexity (FLOPs and Parameters),

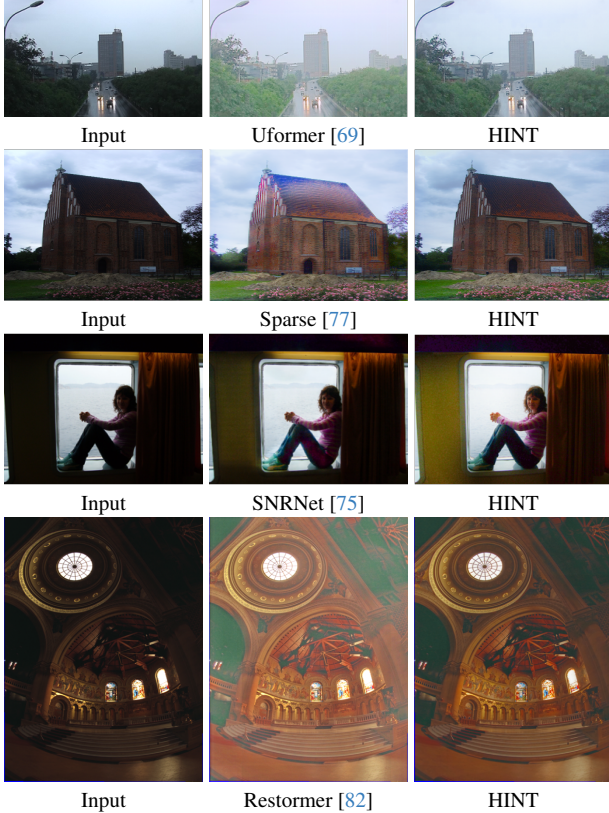


Figure 8. Visualizations on the real-world benchmarks, including NPE [65], DICM[31], VV [61], and MEF [46] (top to bottom). HINT restores a pleasant result, whereas the considered technologies meet under-/over-exposed problem [75, 82], or trigger color distortion [77], or remain significant artifacts [69].

latency (Run-times), and performance (PSNR), as shown in Table 7. HINT obtains the highest PSNR score, while maintaining lower model complexity than CNN-based MIR-Net [81], Transformer-based IPT [3] and Restormer [82].

Evaluation on real-world scenarios. To assess the performance of HINT under real-world scenarios, we test it on real-world dataset without ground-truth, including DICM [31], MEF [46], NPE [65], and VV [61]. The quantitative comparisons are summarized in Table 8, where HINT outperforms all other methods. Furthermore, as shown in Figure 8, HINT restores a visually pleasing restoration, whereas the considered technologies meet under-/over-exposed problem [75, 82], trigger color distortion [77], or remain significant artifacts [69].

Application to high-level vision Task. We conduct the low-light object detection experiment on the ExDark [44] dataset. HINT is pre-trained on the LOL-v2-syn subset and directly applied to enhance the low-light images, with the YOLO-v3 [53] model serving as the detector. The enhanced images bring benefits for the downstream task in qualitative (Figure 9) and quantitative ways (Table 9).

Table 9. Quantitative result of low-light object detection Ex-Dark [44] benchmark. HINT positively impacts the downstream task, and boosts the average precision (AP) scores to 7.6%.

Metric	Input	HINT	Δ
Mean (average precision, AP)	45.1	52.7	+7.6



Figure 9. Visual comparison of low-light object detection. Compared to the low-light input (left), the detector can predict a well-placed bounding box on the image restored by HINT (right).



Figure 10. Failure Case. HINT, which is pre-trained on the synthetic dataset, meets the challenges of restoring input under extremely low-light conditions.

5. Conclusion

We present HINT, a Transformer-based pipeline for image restoration. Without bells and whistles, HINT is simple yet effective for 5 typical restoration tasks on 12 benchmarks, which demonstrates the effect of two design choices: 1) Hierarchical Multi-Head Attention (HMHA); 2) Query-Key Cache Updating (QKCU). By leveraging HMHA to migrate redundancy that is rooted in the vanilla Multi-Head Attention (MHA), and introducing QKCU to enhance interactions between heads via intra- and inter- modulation, HINT is able to perform favorably against previous state-of-the-art algorithms in terms of model complexity and accuracy. To the best of our knowledge, HINT is the first work to restore high-quality images by exploring an efficient MHA mechanism within the widely-used Transformer architecture. This work provides a promising direction to achieve superior restoration performance, and we hope this community can ignite the interest and benefit from it.

Limitations. While HINT offers a plausible solution for image restoration, an interesting way to achieve better results is to solve the failure case it triggers. As shown in Figure 10, HINT struggles to recover some cases under extremely low-light conditions. One potential reason for this could be the domain gap between the synthetic datasets used for pre-training and real-world data. Collecting large-scale real-world datasets for further training could be a valuable direction for future work.

References

- [1] Karim Ahmed, Nitish Shirish Keskar, and Richard Socher. Weighted transformer network for machine translation. *arXiv preprint arXiv:1711.02132*, 2017. 3
- [2] Yuanhao Cai, Hao Bian, Jing Lin, Haoqian Wang, Radu Timofte, and Yulun Zhang. Retinexformer: One-stage retinex-based transformer for low-light image enhancement. In *ICCV*, 2023. 1, 2, 5
- [3] Hanting Chen, Yunhe Wang, Tianyu Guo, Chang Xu, Yiping Deng, Zhenhua Liu, Siwei Ma, Chunjing Xu, Chao Xu, and Wen Gao. Pre-trained image processing transformer. In *CVPR*, 2021. 2, 3, 7, 8
- [4] Liangyu Chen, Xiaojie Chu, Xiangyu Zhang, and Jian Sun. Simple baselines for image restoration. In *ECCV*, 2022. 5, 6
- [5] Tao Chen, Xiruo Jiang, Gensheng Pei, Zeren Sun, Yucheng Wang, and Yazhou Yao. Knowledge transfer with simulated inter-image erasing for weakly supervised semantic segmentation. In *ECCV*, 2024. 2
- [6] Wei-Ting Chen, Hao-Yu Fang, Jian-Jiun Ding, Cheng-Che Tsai, and Sy-Yen Kuo. Jstasr: Joint size and transparency-aware snow removal algorithm based on modified partial convolution and veiling effect removal. In *ECCV*, 2020. 5, 6
- [7] Wei-Ting Chen, Hao-Yu Fang, Cheng-Lin Hsieh, Cheng-Che Tsai, I Chen, Jian-Jiun Ding, Sy-Yen Kuo, et al. All snow removed: Single image desnowing algorithm using hierarchical dual-tree complex wavelet representation and contradict channel loss. In *ICCV*, 2021. 5, 6
- [8] Xiang Chen, Hao Li, Mingqiang Li, and Jinshan Pan. Learning a sparse transformer network for effective image deraining. In *CVPR*, 2023. 3
- [9] Sunghyun Cho and Seungyong Lee. Fast motion deblurring. *ACM TOG*, 28(5):1–8, 2009. 2
- [10] Sung-Jin Cho, Seo-Won Ji, Jun-Pyo Hong, Seung-Won Jung, and Sung-Jea Ko. Rethinking coarse-to-fine approach in single image deblurring. In *ICCV*, 2021. 2
- [11] Marcos V Conde, Gregor Geigle, and Radu Timofte. Instruc-tir: High-quality image restoration following human instructions. In *ECCV*, 2024. 6
- [12] Jean-Baptiste Cordonnier, Andreas Loukas, and Martin Jaggi. Multi-head attention: Collaborate instead of concatenate. *arXiv preprint arXiv:2006.16362*, 2020. 3
- [13] Yuning Cui, Wenqi Ren, Xiaochun Cao, and Alois Knoll. Focal network for image restoration. In *ICCV*, 2023. 5, 6
- [14] Yuning Cui, Yi Tao, Zhenshan Bing, Wenqi Ren, Xinwei Gao, Xiaochun Cao, Kai Huang, and Alois Knoll. Selective frequency network for image restoration. In *ICLR*, 2023. 5, 6
- [15] Yuning Cui, Wenqi Ren, Xiaochun Cao, and Alois Knoll. Image restoration via frequency selection. *TPAMI*, 46(2): 1093–1108, 2024. 6
- [16] Yuning Cui, Syed Waqas Zamir, Salman Khan, Alois Knoll, Mubarak Shah, and Fahad Shahbaz Khan. AdaIR: Adaptive all-in-one image restoration via frequency mining and modulation. In *ICLR*, 2025. 6
- [17] Xin Deng and Pier Luigi Dragotti. Deep convolutional neural network for multi-modal image restoration and fusion. *TPAMI*, 43(10):3333–3348, 2021. 2
- [18] Yu Dong, Yihao Liu, He Zhang, Shifeng Chen, and Yu Qiao. Fd-gan: Generative adversarial networks with fusion-discriminator for single image dehazing. In *AAAI*, 2020. 6
- [19] Alexey Dosovitskiy, Lucas Beyer, Alexander Kolesnikov, Dirk Weissenborn, Xiaohua Zhai, Thomas Unterthiner, Mostafa Dehghani, Matthias Minderer, Georg Heigold, Sylvain Gelly, Jakob Uszkoreit, and Neil Houlsby. An image is worth 16x16 words: Transformers for image recognition at scale. In *ICLR*, 2021. 1, 2, 4
- [20] Kaiwen Duan, Song Bai, Lingxi Xie, Honggang Qi, Qingming Huang, and Qi Tian. Centernet++ for object detection. *TPAMI*, 46(5):3509–3521, 2024. 2
- [21] Rob Fergus, Barun Singh, Aaron Hertzmann, Sam T. Roweis, and William T. Freeman. Removing camera shake from a single photograph. *ACM TOG*, 25(3):787–794, 2006. 2
- [22] Xueyang Fu, Jie Xiao, Yurui Zhu, Aiping Liu, Feng Wu, and Zheng-Jun Zha. Continual image deraining with hypergraph convolutional networks. *TPAMI*, 45(8):9534–9551, 2023. 2
- [23] Shuhang Gu, Yawei Li, Luc Van Gool, and Radu Timofte. Self-guided network for fast image denoising. In *ICCV*, 2019. 2
- [24] Hang Guo, Jinmin Li, Tao Dai, Zhihao Ouyang, Xudong Ren, and Shu-Tao Xia. Mambair: A simple baseline for image restoration with state-space model. In *ECCV*, 2024. 5
- [25] Kaiming He, Jian Sun, and Xiaoou Tang. Single image haze removal using dark channel prior. *TPAMI*, 33(12):2341–2353, 2010. 2
- [26] Dan Hendrycks and Kevin Gimpel. Gaussian error linear units (gelus). *arXiv preprint arXiv:1606.08415*, 2016. 4
- [27] Yifan Jiang, Xinyu Gong, Ding Liu, Yu Cheng, Chen Fang, Xiaohui Shen, Jianchao Yang, Pan Zhou, and Zhangyang Wang. Enlightengan: Deep light enhancement without paired supervision. *TIP*, 30:2340–2349, 2021. 5
- [28] Chanyoung Kim, Woojung Han, Dayun Ju, and Seong Jae Hwang. EAGLE: eigen aggregation learning for object-centric unsupervised semantic segmentation. In *CVPR*, 2024. 2
- [29] Lingshun Kong, Jiangxin Dong, Jianjun Ge, Mingqiang Li, and Jinshan Pan. Efficient frequency domain-based transformers for high-quality image deblurring. In *CVPR*, 2023. 3
- [30] Orest Kupyn, Tetiana Martyniuk, Junru Wu, and Zhangyang Wang. Deblurgan-v2: Deblurring (orders-of-magnitude) faster and better. In *ICCV*, 2019. 2
- [31] Chulwoo Lee, Chul Lee, and Chang-Su Kim. Contrast enhancement based on layered difference representation of 2d histograms. *TIP*, 22(12):5372–5384, 2013. 7, 8
- [32] Boyi Li, Xiulian Peng, Zhangyang Wang, Jizheng Xu, and Dan Feng. Aod-net: All-in-one dehazing network. In *ICCV*, 2017. 2
- [33] Boyi Li, Wenqi Ren, Dengpan Fu, Dacheng Tao, Dan Feng, Wenjun Zeng, and Zhangyang Wang. Benchmarking single-image dehazing and beyond. *TIP*, 28(1):492–505, 2018. 6
- [34] Boyun Li, Xiao Liu, Peng Hu, Zhongqin Wu, Jiancheng Lv, and Xi Peng. All-in-one image restoration for unknown corruption. In *CVPR*, 2022. 6

- [35] Jian Li, Baosong Yang, Zi-Yi Dou, Xing Wang, Michael R Lyu, and Zhaopeng Tu. Information aggregation for multi-head attention with routing-by-agreement. In *NAACL*, 2019. 3
- [36] Ruoteng Li, Robby T. Tan, and Loong-Fah Cheong. All in one bad weather removal using architectural search. In *CVPR*, 2020. 5, 6
- [37] Jingyun Liang, Jiezhong Cao, Guolei Sun, Kai Zhang, Luc Van Gool, and Radu Timofte. Swinir: Image restoration using swin transformer. In *ICCV Workshops*, 2021. 1, 2, 3, 4
- [38] Ding Liu, Bihan Wen, Yuchen Fan, Chen Change Loy, and Thomas S Huang. Non-local recurrent network for image restoration. In *NeurIPS*, 2018. 2
- [39] Risheng Liu, Long Ma, Jiaao Zhang, Xin Fan, and Zhongxuan Luo. Retinex-inspired unrolling with cooperative prior architecture search for low-light image enhancement. In *CVPR*, 2021. 5, 6
- [40] Xing Liu, Masanori Suganuma, Zhun Sun, and Takayuki Okatani. Dual residual networks leveraging the potential of paired operations for image restoration. In *CVPR*, 2019. 2
- [41] Xiaoyu Liu, Jiahao Su, and Furong Huang. Tuformer: Data-driven design of transformers for improved generalization or efficiency. In *ICLR*, 2022. 3, 7
- [42] Yun-Fu Liu, Da-Wei Jaw, Shih-Chia Huang, and Jenq-Neng Hwang. Desnownet: Context-aware deep network for snow removal. *TIP*, 27(6):3064–3073, 2018. 5, 6
- [43] Ze Liu, Yutong Lin, Yue Cao, Han Hu, Yixuan Wei, Zheng Zhang, Stephen Lin, and Baining Guo. Swin transformer: Hierarchical vision transformer using shifted windows. In *ICCV*, 2021. 2
- [44] Yuen Peng Loh and Chee Seng Chan. Getting to know low-light images with the exclusively dark dataset. *CVIU*, 178: 30–42, 2019. 8
- [45] Fangzhou Luo, Xiaolin Wu, and Yanhui Guo. Functional neural networks for parametric image restoration problems. In *NeurIPS*, 2021. 2
- [46] Kede Ma, Kai Zeng, and Zhou Wang. Perceptual quality assessment for multi-exposure image fusion. *TIP*, 24(11): 3345–3356, 2015. 7, 8
- [47] Paul Michel, Omer Levy, and Graham Neubig. Are sixteen heads really better than one? In *NeurIPS*, 2019. 2
- [48] Tan Nguyen, Tam Nguyen, Hai Do, Khai Nguyen, Vishwanath Saragadam, Minh Pham, Khuong Duy Nguyen, Nhat Ho, and Stanley Osher. Improving transformer with an admixture of attention heads. In *NeurIPS*, 2022. 2, 3
- [49] Tam Minh Nguyen, Tan Minh Nguyen, Dung D. D. Le, Duy Khuong Nguyen, Viet-Anh Tran, Richard Baraniuk, Nhat Ho, and Stanley Osher. Improving transformers with probabilistic attention keys. In *ICML*, 2022. 2
- [50] Vaishnav Potlapalli, Syed Waqas Zamir, Salman H Khan, and Fahad Shahbaz Khan. Promptir: Prompting for all-in-one image restoration. In *NeurIPS*, 2023. 6
- [51] Kuldeep Purohit, Maitreya Suin, AN Rajagopalan, and Vishnu Naresh Boddeti. Spatially-adaptive image restoration using distortion-guided networks. In *ICCV*, 2021. 2
- [52] Yanyun Qu, Yizi Chen, Jingying Huang, and Yuan Xie. Enhanced pix2pix dehazing network. In *CVPR*, 2019. 6
- [53] Joseph Redmon. Yolov3: An incremental improvement. *arXiv preprint arXiv:1804.02767*, 2018. 8
- [54] Noam Shazeer, Zhenzhong Lan, Youlong Cheng, Nan Ding, and Le Hou. Talking-heads attention. *arXiv preprint arXiv:2003.02436*, 2020. 3
- [55] Xibin Song, Dingfu Zhou, Wei Li, Yuchao Dai, Zhelun Shen, Liangjun Zhang, and Hongdong Li. Tusr-net: Triple unfolding single image dehazing with self-regularization and dual feature to pixel attention. *TIP*, 32:1231–1244, 2023. 2
- [56] Yuda Song, Zhuqing He, Hui Qian, and Xin Du. Vision transformers for single image dehazing. *TIP*, 32:1927–1941, 2023. 2, 6
- [57] Fu-Jen Tsai, Yan-Tsung Peng, Yen-Yu Lin, Chung-Chi Tsai, and Chia-Wen Lin. Stripformer: Strip transformer for fast image deblurring. In *ECCV*, 2022. 1, 2
- [58] Jeya Maria Jose Valanarasu, Rajeev Yasarla, and Vishal M. Patel. Transweather: Transformer-based restoration of images degraded by adverse weather conditions. In *CVPR*, 2022. 5, 6
- [59] Ashish Vaswani, Noam Shazeer, Niki Parmar, Jakob Uszkoreit, Llion Jones, Aidan N Gomez, Łukasz Kaiser, and Illia Polosukhin. Attention is all you need. In *NeurIPS*, 2017. 1, 2, 4
- [60] Elena Voita, David Talbot, Fedor Moiseev, Rico Sennrich, and Ivan Titov. Analyzing multi-head self-attention: Specialized heads do the heavy lifting, the rest can be pruned. In *ACL*, 2019. 2
- [61] Vassilios Vonikakis, Rigas Kouskouridas, and Antonios Gasteratos. On the evaluation of illumination compensation algorithms. *MTA*, 77:9211–9231, 2018. 7, 8
- [62] Yuning Cui, Wenqi Ren, Xiaochun Cao, and Alois Knoll. Revitalizing convolutional network for image restoration. *TPAMI*, 46(12):9423–9438, 2024. 5, 6
- [63] Cong Wang, Jinshan Pan, Wei Wang, Jiangxin Dong, Mengzhu Wang, Yakun Ju, and Junyang Chen. Promptrestorer: A prompting image restoration method with degradation perception. In *NeurIPS*, 2023. 5
- [64] Huadong Wang, Xin Shen, Mei Tu, Yimeng Zhuang, and Zhiyuan Liu. Improved transformer with multi-head dense collaboration. *TASLP*, 30:2754–2767, 2022. 2, 3
- [65] Shuhang Wang, Jin Zheng, Hai-Miao Hu, and Bo Li. Naturalness preserved enhancement algorithm for non-uniform illumination images. *TIP*, 22(9):3538–3548, 2013. 7, 8
- [66] Tianyu Wang, Xin Yang, Ke Xu, Shaozhe Chen, Qiang Zhang, and Rynson WH Lau. Spatial attentive single-image deraining with a high quality real rain dataset. In *CVPR*, 2019. 2, 7
- [67] Wenjing Wang, Huan Yang, Jianlong Fu, and Jiaying Liu. Zero-reference low-light enhancement via physical quadruple priors. In *CVPR*, 2024. 5
- [68] Zhou Wang, Alan C Bovik, Hamid R Sheikh, and Eero P Simoncelli. Image quality assessment: from error visibility to structural similarity. *TIP*, 13(4):600–612, 2004. 5
- [69] Zhendong Wang, Xiaodong Cun, Jianmin Bao, Wengang Zhou, Jianzhuang Liu, and Houqiang Li. Uformer: A gen-

- eral u-shaped transformer for image restoration. In *CVPR*, 2022. 2, 5, 6, 7, 8
- [70] Chen Wei, Wenjing Wang, Wenhan Yang, and Jiaying Liu. Deep retinex decomposition for low-light enhancement. In *BMVC*, 2018. 2
- [71] Yanjie Wen, Ping Xu, Zhihong Li, and Wangtu Xu(ATO). An illumination-guided dual attention vision transformer for low-light image enhancement. *PR*, 158:111033, 2025. 5
- [72] Jiangwei Weng, Zhiqiang Yan, Ying Tai, Jianjun Qian, Jian Yang, and Jun Li. Mamballie: Implicit retinex-aware low light enhancement with global-then-local state space. In *NeurIPS*, 2024. 5
- [73] Da Xiao, Qingye Meng, Shengping Li, and Xingyuan Yuan. Improving transformers with dynamically composable multi-head attention. In *ICML*, 2024. 2, 3
- [74] Jie Xiao, Xueyang Fu, Aiping Liu, Feng Wu, and Zheng-Jun Zha. Image de-raining transformer. *TPAMI*, 45(11):12978–12995, 2023. 2
- [75] Xiaogang Xu, Ruixing Wang, Chi-Wing Fu, and Jiaya Jia. Snr-aware low-light image enhancement. In *CVPR*, 2022. 2, 5, 7, 8
- [76] Sidi Yang, Tianhe Wu, Shuwei Shi, Shanshan Lao, Yuan Gong, Mingdeng Cao, Jiahao Wang, and Yujiu Yang. Maniqa: Multi-dimension attention network for no-reference image quality assessment. In *CVPR*, 2022. 5, 7
- [77] Wenhan Yang, Wenjing Wang, Haofeng Huang, Shiqi Wang, and Jiaying Liu. Sparse gradient regularized deep retinex network for robust low-light image enhancement. *TIP*, 30: 2072–2086, 2021. 5, 6, 7, 8
- [78] Mingde Yao, Ruikang Xu, Yuanshen Guan, Jie Huang, and Zhiwei Xiong. Neural degradation representation learning for all-in-one image restoration. *TIP*, 33:5408–5423, 2024. 6
- [79] Ke Yu, Xintao Wang, Chao Dong, Xiaoou Tang, and Chen Change Loy. Path-restore: Learning network path selection for image restoration. *TPAMI*, 44(10):7078–7092, 2022. 2
- [80] Zongsheng Yue, Qian Zhao, Lei Zhang, and Deyu Meng. Dual adversarial network: Toward real-world noise removal and noise generation. In *ECCV*, 2020. 2
- [81] Syed Waqas Zamir, Aditya Arora, Salman Khan, Munawar Hayat, Fahad Shahbaz Khan, Ming-Hsuan Yang, and Ling Shao. Learning enriched features for real image restoration and enhancement. In *ECCV*, 2020. 5, 6, 7, 8
- [82] Syed Waqas Zamir, Aditya Arora, Salman Khan, Munawar Hayat, Fahad Shahbaz Khan, and Ming-Hsuan Yang. Restormer: Efficient transformer for high-resolution image restoration. In *CVPR*, 2022. 1, 2, 3, 4, 5, 6, 7, 8
- [83] Syed Waqas Zamir, Aditya Arora, Salman Khan, Munawar Hayat, Fahad Shahbaz Khan, Ming-Hsuan Yang, and Ling Shao. Learning enriched features for fast image restoration and enhancement. *TPAMI*, 45(2):1934–1948, 2023. 2
- [84] Xiangyu Zhang, Xinyu Zhou, Mengxiao Lin, and Jian Sun. Shufflenet: An extremely efficient convolutional neural network for mobile devices. In *CVPR*, 2018. 7
- [85] Xiaofeng Zhang, Yikang Shen, Zeyu Huang, Jie Zhou, Wenge Rong, and Zhang Xiong. Mixture of attention heads: Selecting attention heads per token. In *EMNLP*, 2022. 3
- [86] Yulun Zhang, Kunpeng Li, Kai Li, Bineng Zhong, and Yun Fu. Residual non-local attention networks for image restoration. In *ICLR*, 2019. 2
- [87] Yonghua Zhang, Jiawan Zhang, and Xiaojie Guo. Kindling the darkness: A practical low-light image enhancer. In *ACMMM*, 2019. 5, 6
- [88] Shihao Zhou, Duosheng Chen, Jinshan Pan, Jinglei Shi, and Jufeng Yang. Adapt or perish: Adaptive sparse transformer with attentive feature refinement for image restoration. In *CVPR*, 2024. 3, 4, 5, 6
- [89] Shihao Zhou, Jinshan Pan, Jinglei Shi, Duosheng Chen, Lishen Qu, and Jufeng Yang. Seeing the unseen: A frequency prompt guided transformer for image restoration. In *ECCV*, 2024. 3, 5